Mechanisms for wind direction changes in the very stable boundary layer

D. Finn[1,3], R. M. Eckman[1], Z. Gao[2], H. Liu[2]

Keywords: Intermittent; Low fluxes, Low wind speeds; Meander; Wind shear

For submission: J Appl Meteorol Climatol

[1] NOAA Air Resources Laboratory, Field Research Division, 1750 Foote Dr., Idaho Falls, ID, 83402

[2] Laboratory for Atmospheric Research, Washington State University, Pullman, WA

[3] Corresponding author phone: 208-526-0566, email: dennis.finn@noaa.gov

Abstract

Large, rapid, and intermittent changes in wind direction were commonly observed in low wind speed conditions in the very stable boundary layer during the Project Sagebrush Phase 2 field tracer study. This paper investigates the occurrence and magnitude of these wind direction changes in the very stable boundary layer and explores their associated meteorological factors. The evidence indicates that these wind direction changes are largely restricted to near surface wind speeds less than 1.5 m s^{-1} and are associated with momentum and sensible heat fluxes approaching zero in low wind shear conditions. This results in complete vertical decoupling. They are only weakly dependent on the magnitude of turbulence. The magnitude of the wind direction changes is greatest near the surface and decreases upward.

1. Introduction

Dispersion models normally assume plumes are most narrow in the stable boundary layer, consistent with the idea that the horizontal plume spread, σ_y, is directly related to the typically smaller standard deviation σ_θ of the wind direction. This plume behavior was found to be the case during the classical Project Prairie Grass experiments (Barad 1958a ,b) and a number of subsequent studies (Slade 1968). These results were widely accepted at the time (e.g., Gifford 1961; Turner 1970) and are still featured in EPA guidance documents (EPA 2000) and embedded in the implementation of traditional stability class Gaussian plume models.

There is increasing awareness, however, that observed plumes in stable conditions are often much wider than would be expected if σ_θ is the dominant parameter determining plume width, especially in the very stable boundary layer (vSBL) (Mortarini et al. 2016a). Experiments in the

55 vSBL in the 1970s found that plumes generally subtended more than 90^{o} of arc with plumes
56 occasionally being measured across essentially a full 360^{o} over the course of a one-hour
57 averaging period (Sagendorf and Dickson, 1974). This study is still a benchmark for plume
58 dispersion in the vSBL in low wind conditions (Luhar and Hurley 2012). However, these
59 measurements did not provide any finer temporal resolution on what happened during the one-
60 hour measurement period.
61
62 Recent tracer experiments in the vSBL with low wind speed (U) found small σ_θ on time scales of
63 10-min or less that were comparable to classical results such as Project Prairie Grass (Finn et al.
64 2017; Finn et al submitted). However, the measured horizontal plume spreads were much larger
65 than Project Prairie Grass, usually much greater than 90^{o}. This was reminiscent of the Sagendorf
66 and Dickson (1974) results and much larger than the small measured 10-min σ_θ would suggest.
67 Finn et al. (submitted) found that plumes often traveled in a relatively steady direction in these
68 conditions for up to about one-half hour and then abruptly shifted several tens to over 100
69 degrees on time scales of 10-min or less. The resolution of the tracer measurements prohibited
70 any finer breakdown of the timescales of the plume shifts. Hiscox et al. (2010) observed similar
71 phenomena in lidar measurements of smoke plumes.
72
73 Other investigations of turbulence and meander at low U in the vSBL report complementary
74 findings (Sun et al. 2012; Mortarini et al. 2016a, b). Sun et al. (2012) show examples where wind
75 directions were relatively constant over periods of 10-20 min up to more than an hour but
76 punctuated by large shifts in excess of 100^{o} over short time intervals, sometimes less than 1-2
77 min. Mortarini et al. (2016a) show examples where the wind direction was never steady for

periods greater than a few minutes and exhibited nearly continuous oscillatory behavior. The wind direction changes were commonly 100-200^{o} in magnitude and, again, often occurred in less than 1-2 min. All of these results call into question the presumed linkage between narrow plumes and minimal σ_θ in the vSBL. They also highlight the large, rapid, and intermittent nature of these changes in wind direction in the vSBL. The changes can be oscillatory and quasi-periodic but can also be very irregular and intermittent without a discernible pattern.

Some newer plume models attempt to account for the observations of much broader horizontal plume spreads in light winds in the stable boundary layer (e.g., Cimorelli et al. 2004, 2005; Anfossi et al. 2006; Luhar 2013). Venkatram et al. (2013) attempt to model this situation by weighting plume dispersion between a random state and a Gaussian distribution. However, this is an inherently difficult problem and there is little guidance available for how the details of the observed rapid, episodic plume shifts might be captured.

This paper will examine the occurrence of these rapid, intermittent shifts in wind direction in the vSBL at low U with emphasis on their magnitude and triggering mechanisms. The intent is to provide additional information that can be used for improving the modeling of plume dispersion in these conditions. It expands on the efforts by Mahrt (2007, 2008) and Mortarini et al. (2016a, b) for investigating and quantifying this phenomenon using a new vSBL dataset and a methodology focused on the changes in wind direction.

2. Methodology

100 The data used for this analysis were collected during October, 2016 as part of Phase 2 of Project
101 Sagebrush (PSB2), a field tracer study of plume dispersion in low U conditions conducted at the
102 Idaho National Laboratory (INL) (Finn et al. 2017; Finn et al. submitted). Nine nocturnal periods
103 featuring the common presence of vSBL conditions were selected as case studies. Continuous
104 periods were selected that were dominated by a combination of high bulk Richardson number
105 Ri_b, high Brunt-Väisälä frequencies N, low U, and large magnitude negative net radiation (Rn).
106 Ten-minute average Ri_b and N were calculated using temperature and cup anemometer wind
107 speed measurements from measurements at the 2 and 10 m levels of the 62 m Grid 3 tower
108 (GRI). This was one of the primary towers used during Project Sagebrush and is also part of a
109 permanent observation network (Clawson et al. 2007). The summary of these nine periods is
110 shown in Table 1.
111
112 The terrain is generally open and flat with a grass and sagebrush canopy. Median roughness
113 lengths z_o of 3 and 3.8 cm have been estimated for southwest and northeast winds, respectively.
114 Comprehensive descriptions of all the measurements in PSB2 can be found in Finn et al. (2015,
115 2016, 2017).
116
117 Two sets of sonic anemometer data were utilized in the analysis. The Field Research Division of
118 NOAA fielded six R.M. Young Ultrasonic 81000 anemometers at the 2, 3.7, 9, 16.5, 30 and 60
119 m levels on the Grid 3 tower. Washington State University (WSU) deployed five CSAT3 and
120 CSAT3B anemometers arrayed horizontally across the study area at about 3 m agl, two of which
121 were collocated with IRGA sensors. The raw data were collected at 10 Hz but for this analysis
122 they were averaged to generate 1-s averages of U, vertical velocity w, and temperature, and

where available, pressure. Two minute averaging intervals were used to calculate: the momentum fluxes ($u'w'$ and $v'w'$), sensible heat flux ($w'T'$), turbulent kinetic energy (TKE), the standard deviations of W (σ_w) and temperature (σ_T), and the wind shear between levels on the tower (du/dz, dv/dz). Lower case u, v, and w represent the vector components of wind speed. The key measurement for this analysis is the change in degrees of wind direction between 2-min averaging intervals (ΔWD). The maximum ΔWD was fixed at 180° even if the wind direction rotated through more than 180° in the 2-min interval. For example, if the wind direction rotated counterclockwise from 300° to 40° this was calculated as a 100° ΔWD. An ASC minisodar located 1 km northeast of the tower measured 10-min average wind profiles from 30 m up to 200 m agl at 10 m intervals.

3. Results

Table 1 summarizes the times and some aspects of the meteorology for the selected nighttime periods. The listed starting date and time is always in the evening after sundown and the end time is always given for the following morning prior to sunrise. The net radiation (Rn) is based on the averages of 1-h values covering the listed period. The Brunt-Väisälä frequencies (N) represent averages based on individual 10-min values. It is apparent from the N and Rn averages that the selected periods were generally very stable for extended periods of time. Following Mahrt (2007), V_{meso} and RV_{meso} were calculated for each period shown in Table 1 for a 1-h averaging period with 1-min subrecords. V_{meso} and RV_{meso} are velocity scales that represent the strength of mesoscale flow. The results in Table 1 are similar in magnitude to those reported for CASES-99.

Start Date	Start (MST)	End (MST)	N (s^{-1}) (2,10 m)	Rn (W m^{-2})	Avg. V_{meso} (m s^{-1})	V_{meso} S.D. (m s^{-1})	Avg. RV_{meso}
8-Oct	1900	0700	0.129	-61.0	0.54	0.21	0.84
11-Oct	2300	0700	0.108	-73.6	0.42	0.15	0.40
12-Oct	1900	0700	0.091	-60.2	0.47	0.19	0.73
19-Oct	1900	0700	0.081	-63.4	0.45	0.19	0.50
20-Oct	1900	0700	0.105	-58.1	0.43	0.11	0.83
21-Oct	1900	0700	0.105	-54.2	0.49	0.12	0.60
23-Oct	1900	0700	0.096	-43.3	0.54	0.14	0.66
25-Oct	1900	0700	0.070	-45.8	0.46	0.16	0.88
26-Oct	2130	0530	0.093	-51.4	0.45	0.18	1.30

Table 1. Summary of dates, times, and average N and Rn for the nighttime cases selected. The V_{meso} and RV_{meso} results at 2 m a.g.l. are hourly averages for the complete time periods shown following Mahrt (2007).

Unless denoted otherwise, the times shown in plots represent 1900 MST as hour zero then past midnight to 0700 MST the next morning which is represented as hour 12. Dates have been assigned based on the starting date of the complete 12-h period beginning the evening of the starting date and finishing the morning of the next day.

Figure 1 shows an example 1-s wind direction time series from the October 23 case (October 24, 0300-0700 MST). This illustrates how wind direction changes can be very large and abrupt in these conditions. Similar to the examples shown in Sun et al. (2012) and Mortarini et al. (2016a), there is strong oscillatory behavior with large, abrupt changes in wind direction.

Figure 2 shows the large Ri_b and N for the nine cases selected and highlights their generally strongly stable nature. Figure 3 shows the 2-min ΔWD as a function of U at 2 m agl for all time periods encompassed in Table 1. It is clear that the overall U were generally < 2 m s^{-1} and heavily weighted toward U < 1.5 m s^{-1}. Furthermore, almost all of the large ΔWD had U < 1.5 m s^{-1}.

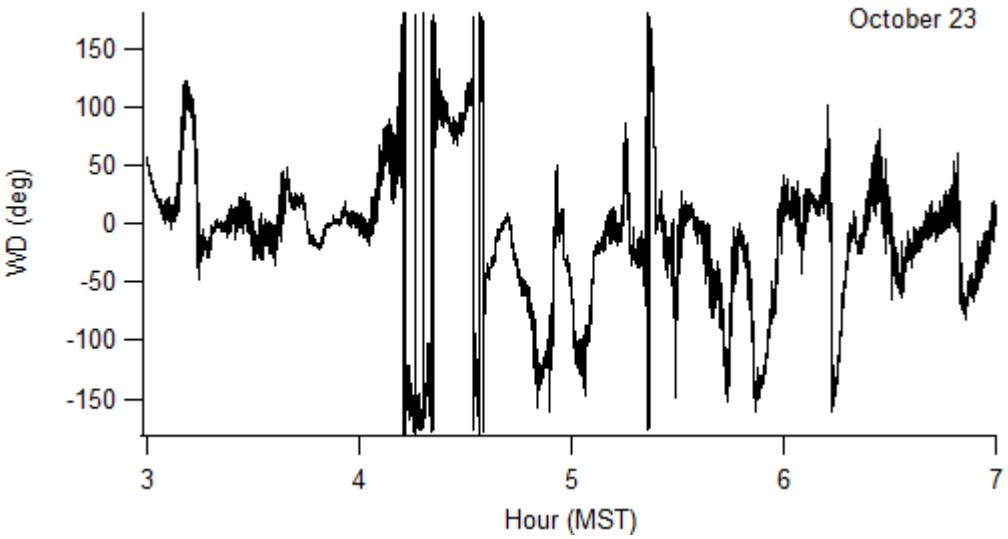

Figure 1. Example 1-s wind direction time series. The wind directions have been rotated from 0 to 360° coordinates to -180° to +180° to minimize frequent wrapping through true north.

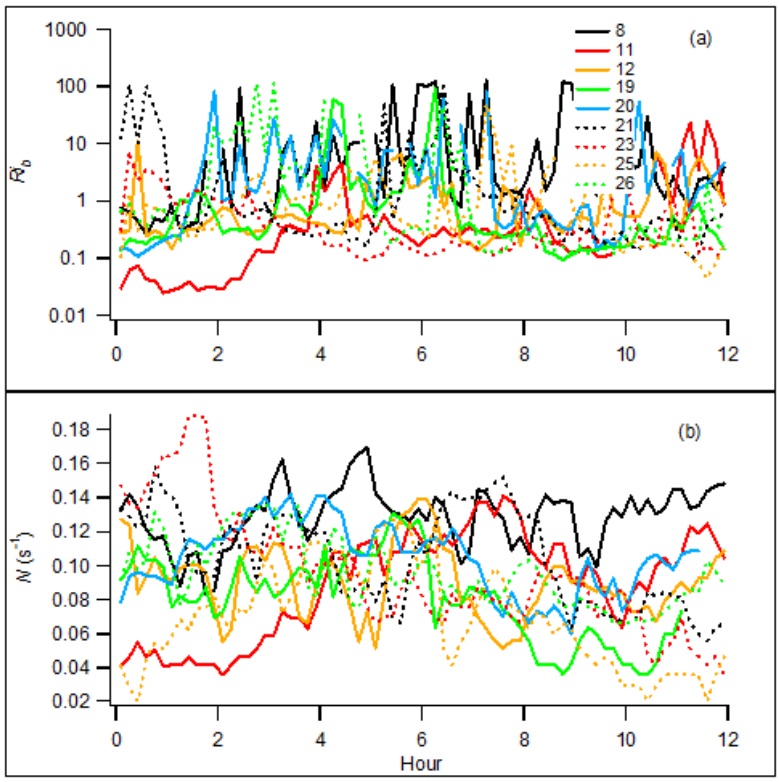

Figure 2. Ten-minute average (a) bulk Richardson number (Ri_b) and (b) Brunt-Väisälä frequency (N) for all times used. The starting October dates are indicated in the legend.

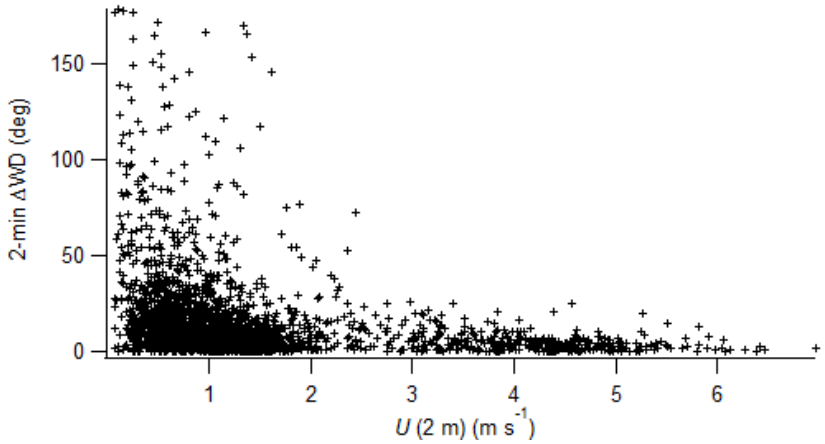

Figure 3. Two-minute ΔWD as a function of *U* at 2 m a.g.l. for all times used.

3.1 Effects of turbulence and turbulent fluxes on ΔWD

Figure 4 summarizes the ΔWD results as a function of the sensible heat and momentum fluxes for all the 2-min periods of Table 1 at four heights on the tower. A salient feature of these plots is how the large ΔWD were, with relatively few exceptions, associated with sensible heat and momentum fluxes near zero. This was true for all levels shown and was especially the case for the momentum fluxes. Large wind shifts therefore appear to be keyed to times with limited vertical transport by turbulence. The aggregate data from the 3 m agl WSU surface array showed very similar patterns. Trini Castelli et al. (2014) observed that the friction velocities and sensible heat fluxes were very small for a suburban site at low *U* in the SBL.

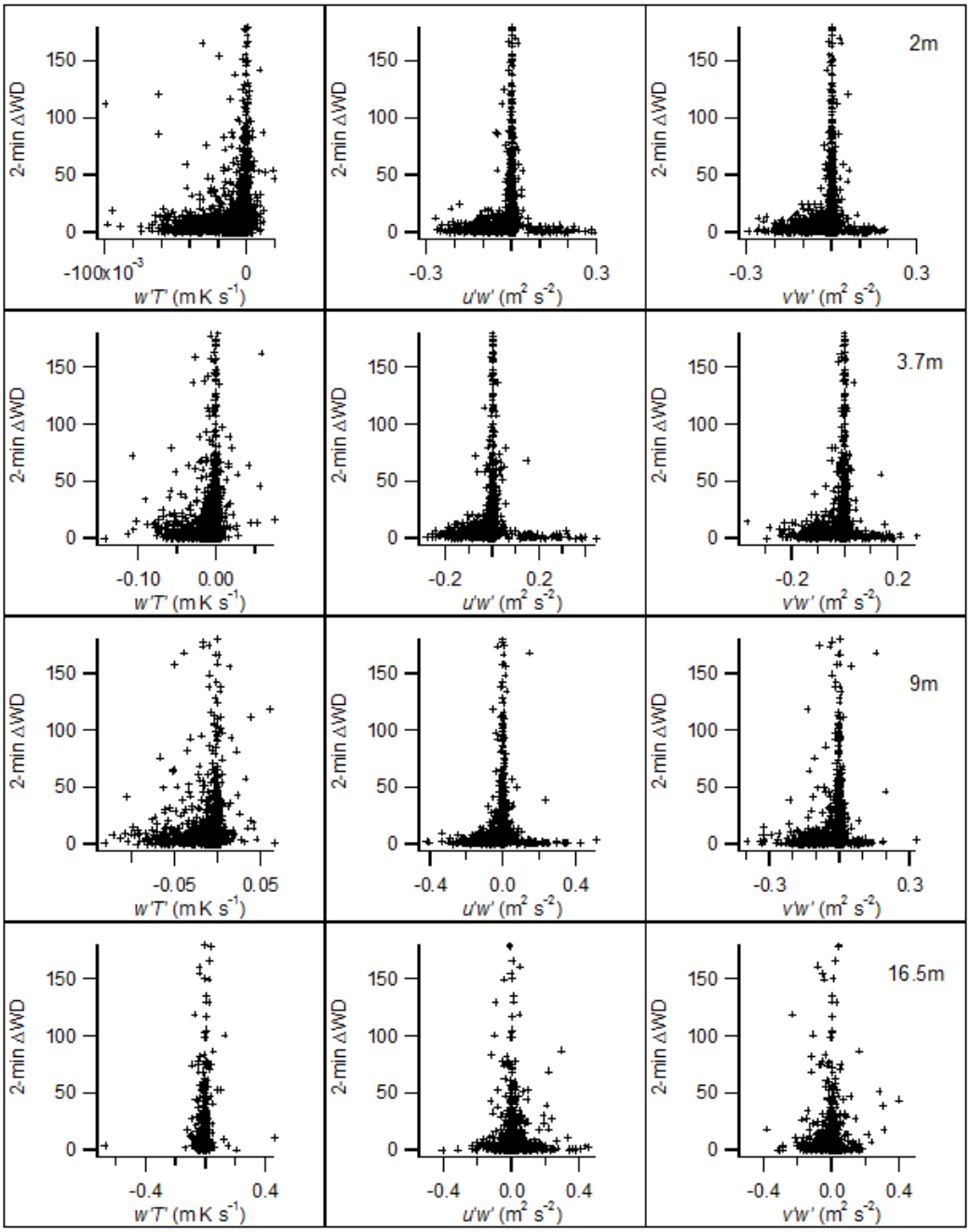

Figure 4. ΔWD results as a function of the sensible heat and momentum fluxes for all the 2-min periods of Table 1 at four heights on the tower.

Similarly, Fig. 5 summarizes the ΔWD results as a function of σ_w, √TKE, and σ_T for all of the 2-min periods. It is clear that increases in ΔWD tended to be associated with low turbulence with ΔWD decreasing as these measures of turbulence increased. Again, the WSU results were similar.

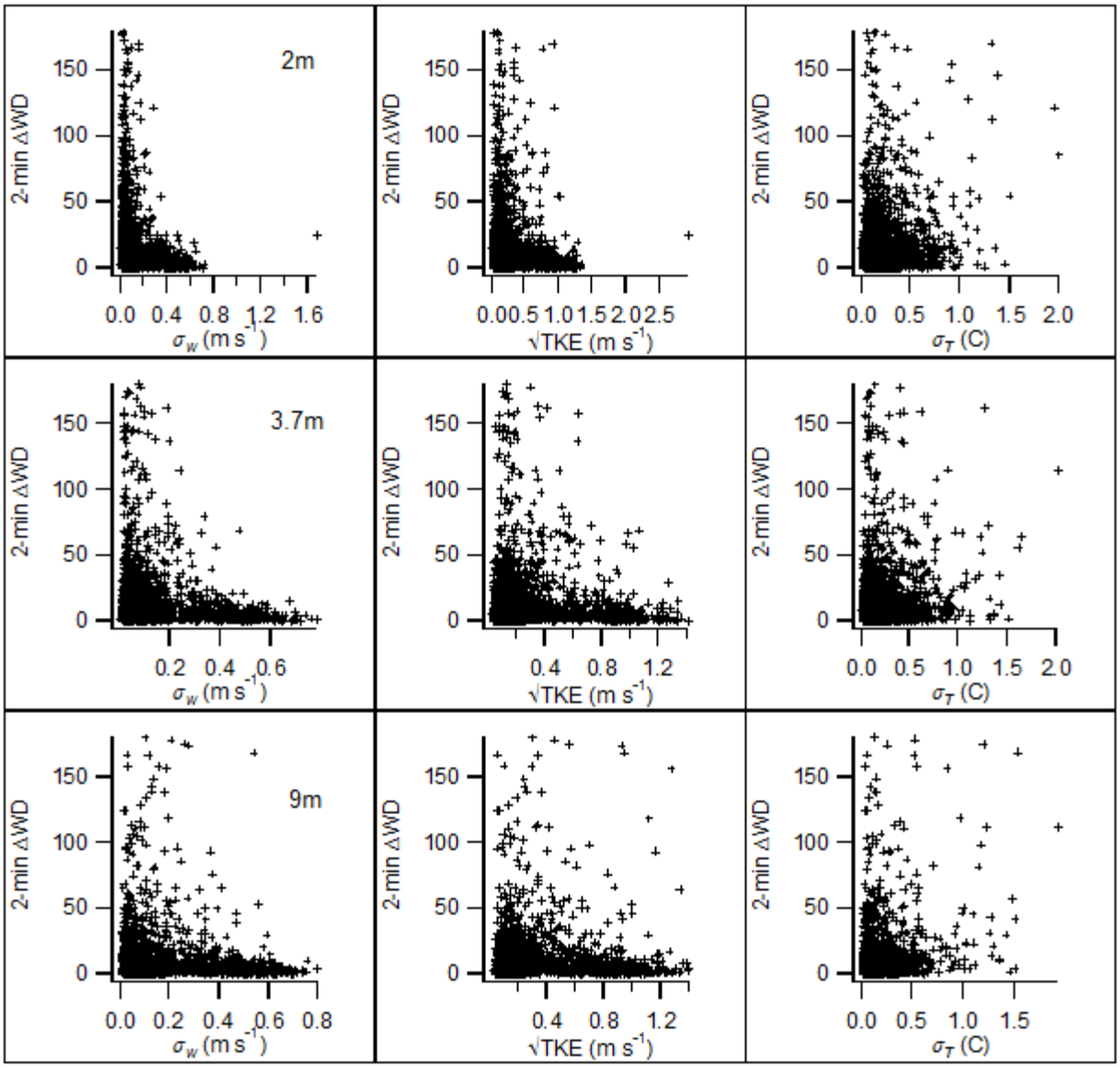

Figure 5. ΔWD results as a function of σ_w, √TKE, and σ_T for all of the 2-min periods included in Table 1.

Results from a subset of the study days will now be shown to provide some details on how ΔWD is affected by factors such as U, height, wind shear, and the presence or absence of low-level jets (LLJ). Extended periods of time from the October 8, 19, 20, 23, and 26 cases are shown in Figs. 6-10, respectively.

200 3.2 Effects of *U* and height on ΔWD

201 One of the most salient features of the data is the not unexpected association between low *U* and
202 increases in ΔWD. This could be extended over periods of time (e.g., Figs. 6, 8, 9, 10) or to more
203 restricted episodes (e.g. hour 6.3, Fig. 7; hours 3.7 and 8.1, Fig. 9). In a separate analysis it was
204 found that periods exhibiting sustained periods of wind direction change in mainly one direction
205 of rotation could be combined to form more or less continuous periods up to a half hour or more
206 where the net change in one direction of rotation was much larger than the individual 2-min
207 changes (up to 540^{o} total). The association between low *U* and ΔWD is consistent with the
208 results shown in Fig. 3. Thus, low *U* is a proximate cause of increased ΔWD.

209

210 Another prominent feature of the data is that the magnitude of ΔWD is related to height (Figs. 6-
211 10, parts (b)). In most cases, large ΔWD were restricted to 16.5 m and below and sometimes only
212 involving the 2 and 3.7 m heights. Figures 8 and 9 show especially limited ΔWD above 9 m.
213 Figure 11 summarizes this dependency on height. The frequency of ΔWD magnitudes are binned
214 in 5^{o} increments and shown as a function of (a) GRI measurement height or (b) surface location.
215 The surface stations had ΔWD between 0 and 5^{o} about 40% of the time with the fraction in this
216 bin increasing upward to over 70% at 60 m agl. Less than 10% of the ΔWD at heights above 30
217 m were > 10^{o}. In contrast, the fraction at surface levels decreased much more slowly and
218 exhibited a distinct increase to 5-8% for ΔWD > 40^{o}.

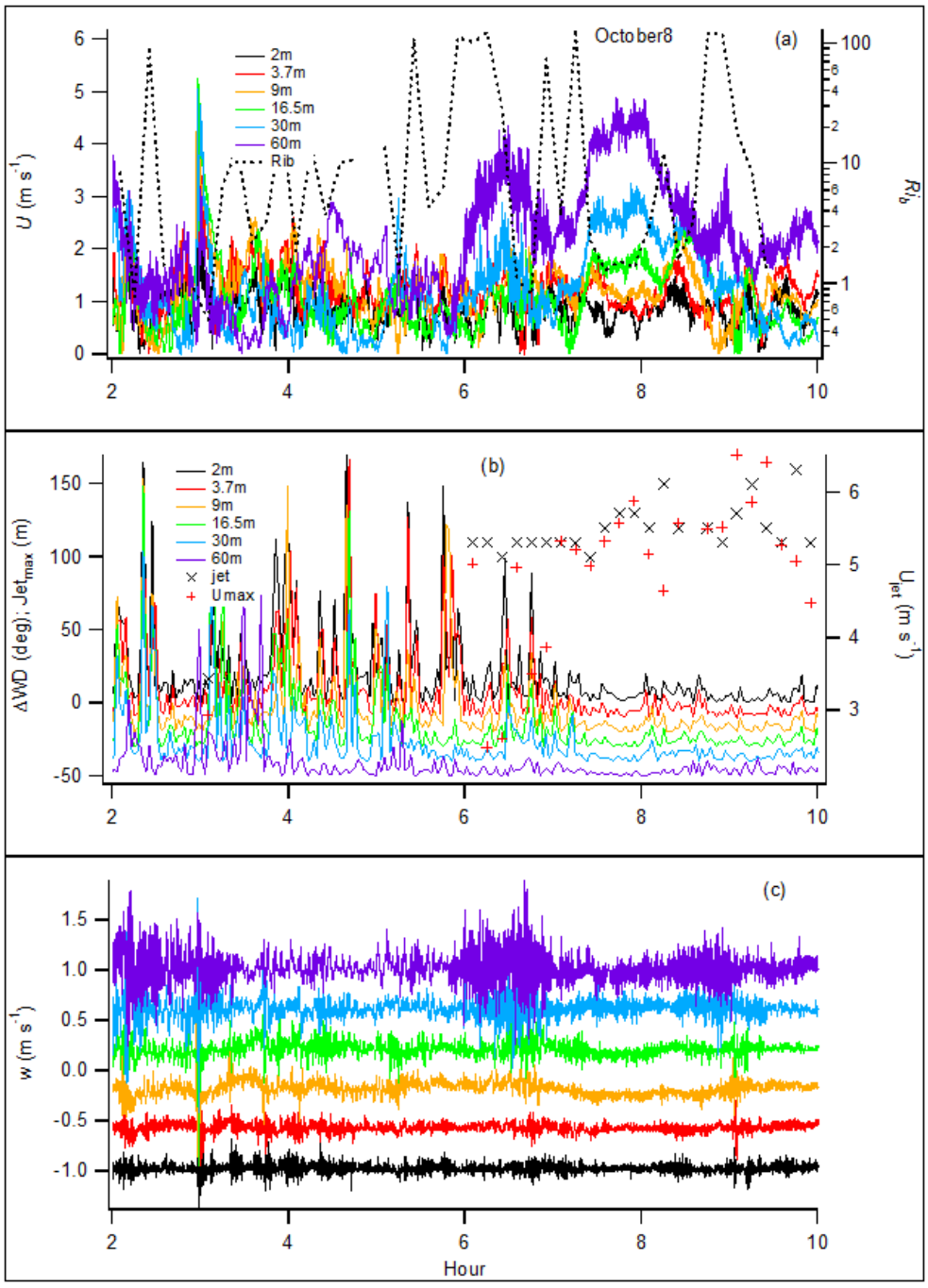

Figure 6. GRI tower October 8: (a) 1-s U and 10-min Ri_b; (b) 2-min ΔWD (-10° offsets for successive heights beginning at 3.7 m) and 10-min LLJ (height and U_{max}); and (c) 1-s vertical velocity w. ΔWD and w traces for adjacent heights are offset for clarity by 10° and 0.4 m s^{-1}, respectively. Hour is time from 1900 MST reference.

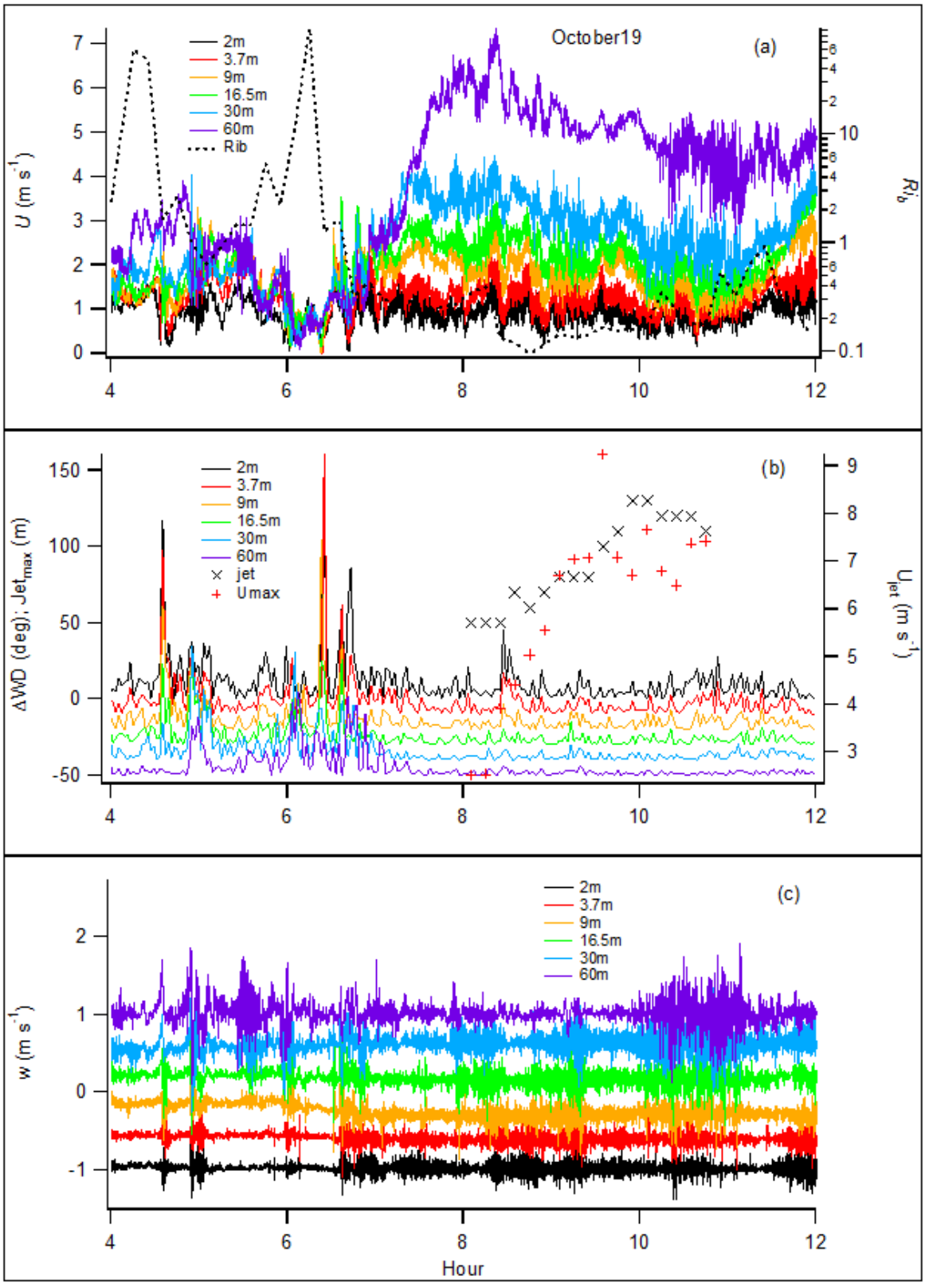

Figure 7. GRI tower October 19 with same caption as Fig. 6.

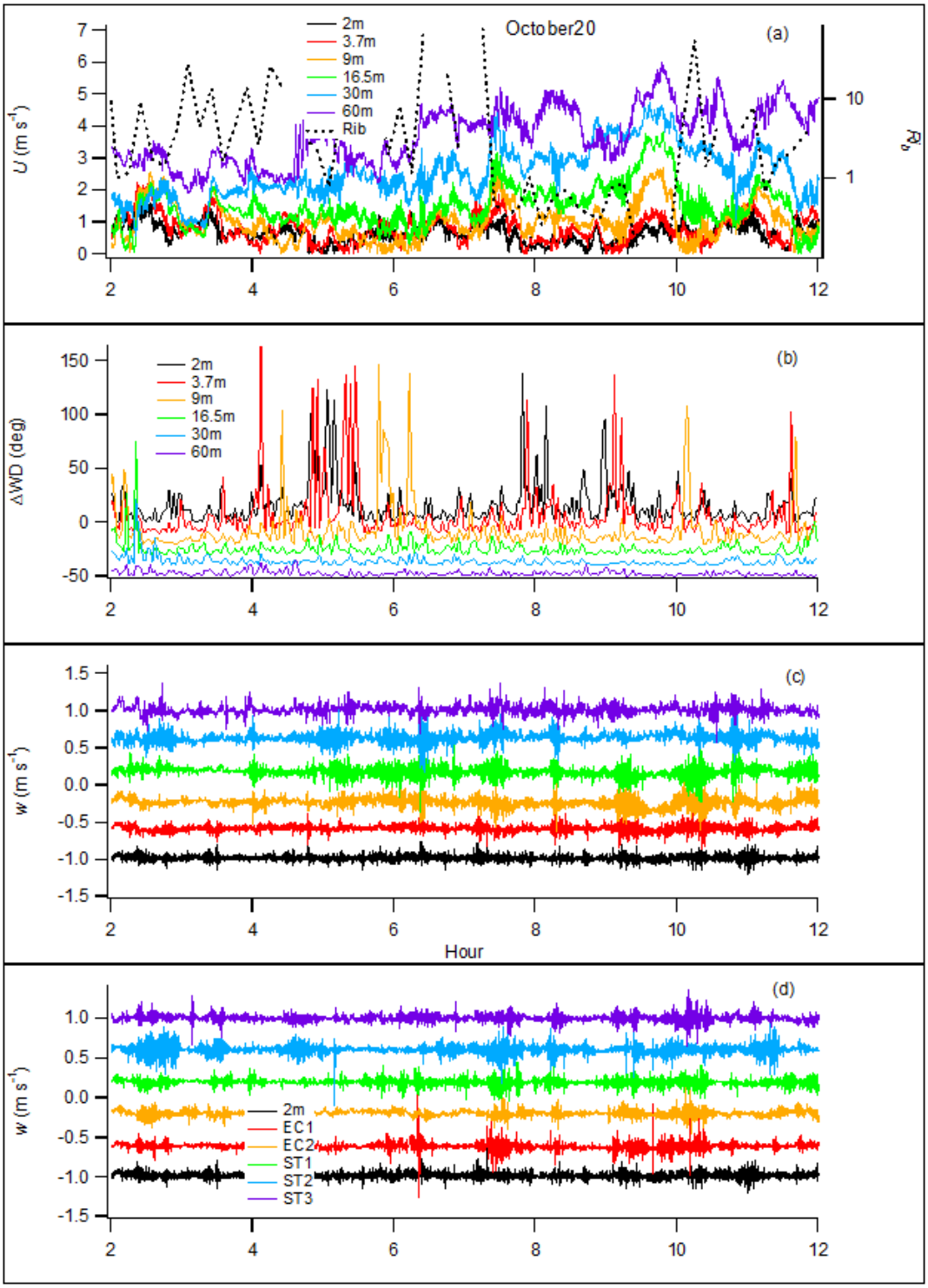

Figure 8. GRI tower October 20: (a) 1-s U and 10-min Ri_b; (b) 2-min ΔWD (-10° offsets for successive heights beginning at 3.7 m) (no LLJ); (c) 1-s vertical velocity W; and (d) 1-sec vertical velocity w measured across surface array. ΔWD and w traces for adjacent heights are offset for clarity by 10° and 0.4 m s^{-1}, respectively. Hour is time from 1900 MST reference.

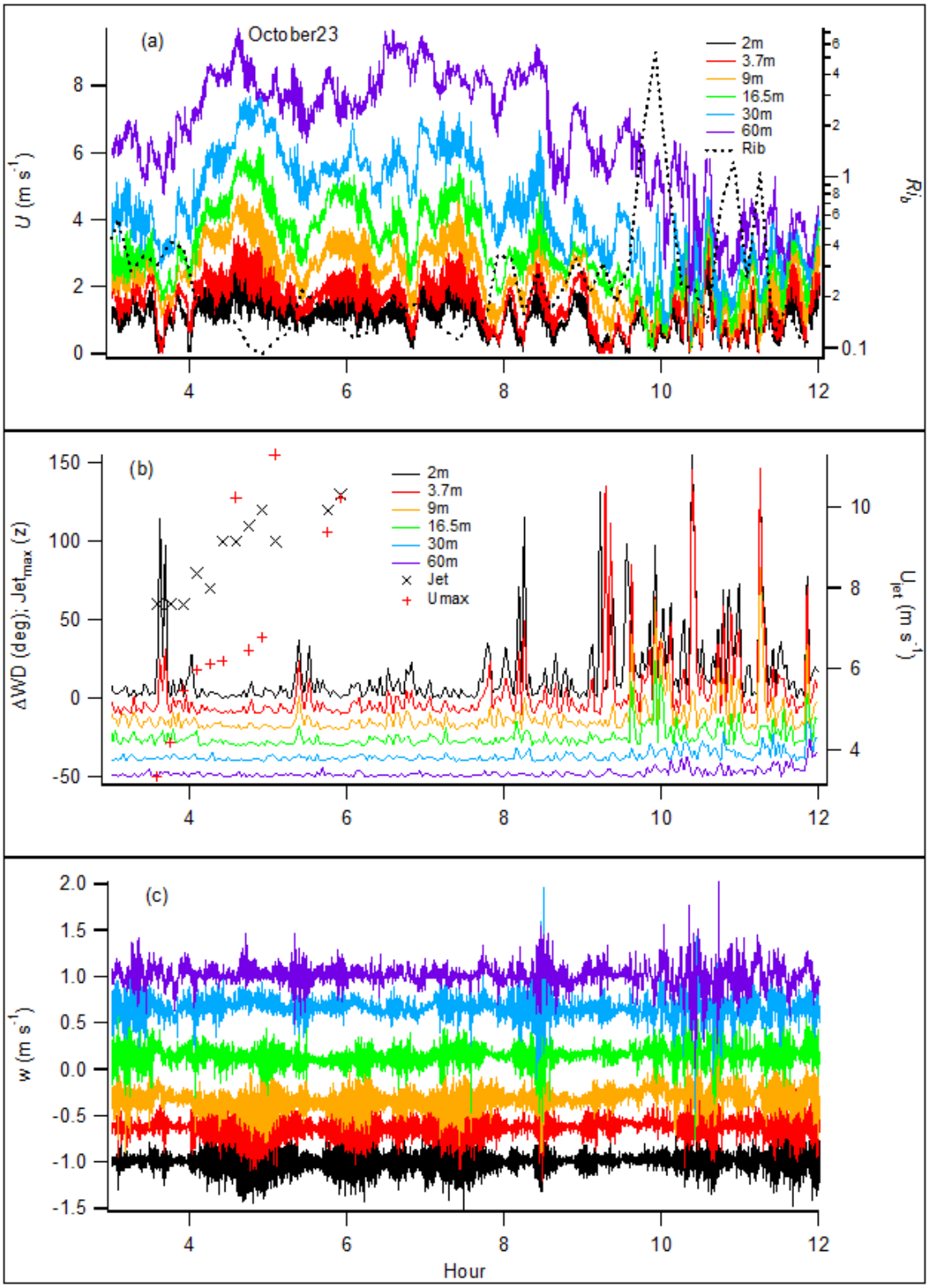

Figure 9. GRI tower October 23 with same caption as Fig. 6.

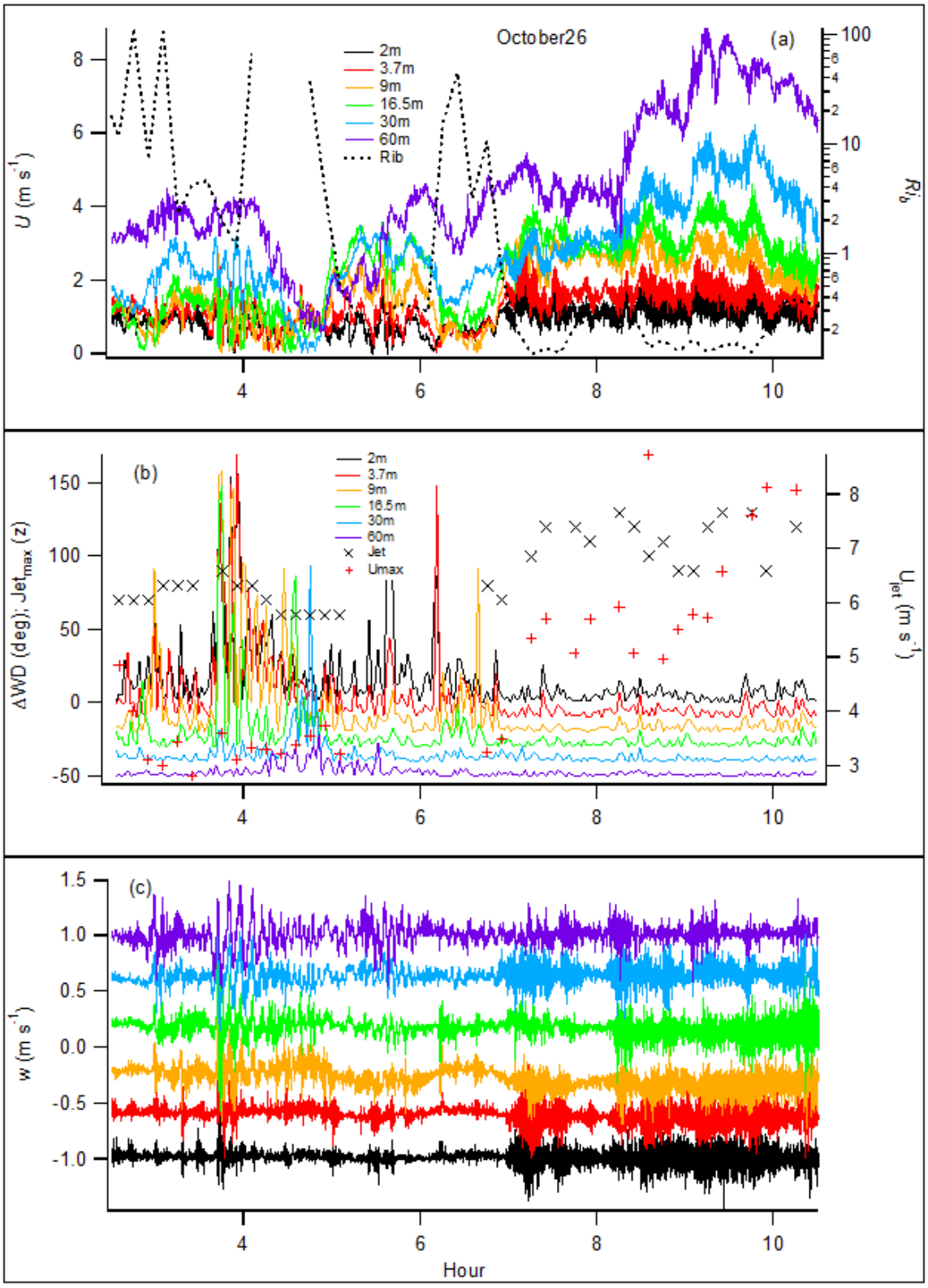

Figure 10. GRI tower October 26 with same caption as Fig. 6.

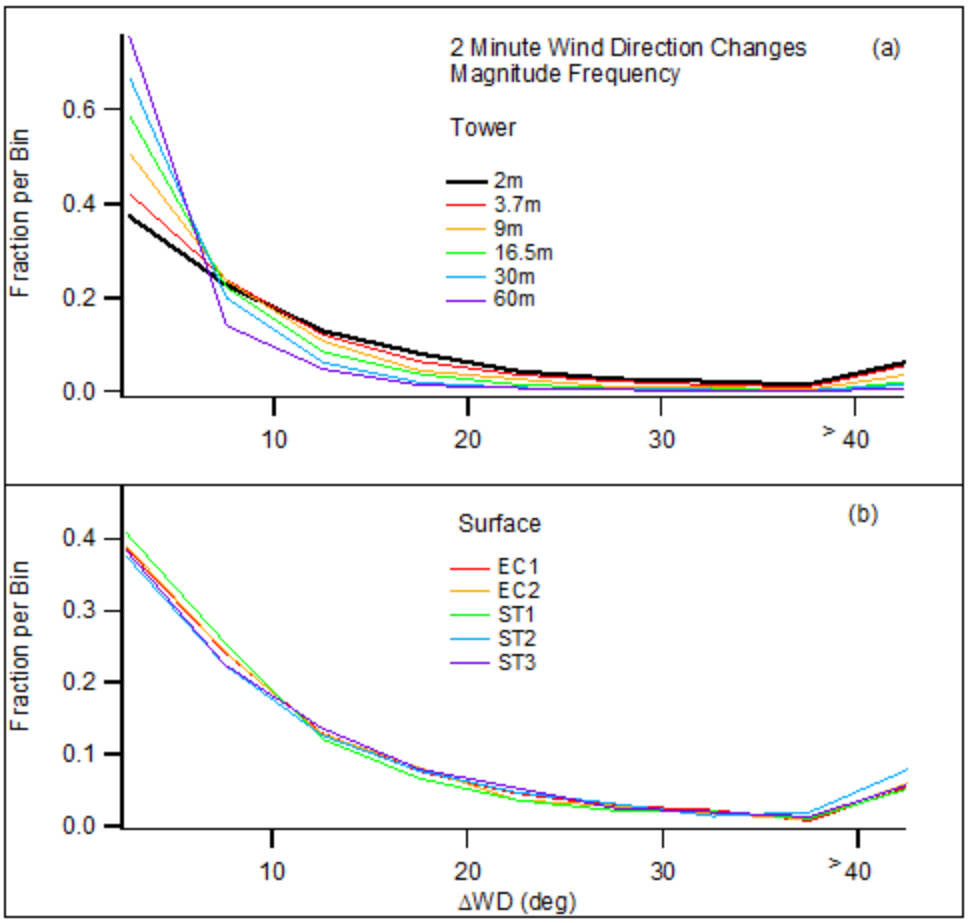

Figure 11. Fraction of 2-min ΔWD changes binned in 5° intervals by (a) height on the GRI tower and (b) the surface array.

3.3 Effect of wind shear on ΔWD

The data also point to the role of wind shear in whether or not large ΔWD developed. It is apparent in Figs. 6-10 that Ri_b was often very large. Periods with high Ri_b were more likely to be associated with periods of larger ΔWD (e.g., Figs. 6, 9, 10) and lower Ri_b were more likely to be associated with lower ΔWD (e.g., Figs. 7, 9, 10). This was generally the case although there were exceptions (e.g., Fig. 6, hour 9). While steep temperature gradients contributed to the large Ri_b, a major reason for the large Ri_b was the often small differences in wind speed between heights resulting in small denominators. As such Ri_b is a proxy for wind shear with lower Ri_b indicating

249 that vertical wind shear tended to suppress ΔWD and the minimization of wind shear (higher Ri_b)
250 tended to promote larger ΔWD. In some instances the wind speed differences in the denominator
251 were zero resulting in occasional missing values for Ri_b (e.g., Figs. 6, 8, 10).
252
253 An example of this from October 23 is shown in Fig. 12. This shows the component *du/dz* and
254 *dv/dz* wind shears between the 2 and 9, 9 and 16.5, and 16.5 and 30 m heights on the tower. The
255 magnitudes of the wind shears were generally > 0.1 s^{-1} until about hour 9. Comparing this result
256 with Fig. 9 it can be seen that this was when the vertical gradient in *U* began to decrease and
257 ΔWD began to increase. Figure 13 aggregates the *du/dz* and *dv/dz* for two levels (2 and 9, 9 and
258 16.5 m) for all of the data in the analysis. While there are exceptions, the majority of the large
259 ΔWD were within ± 0.1 s^{-1}. Levels at 9 m and below had the maximum magnitudes and
260 variability in shear.

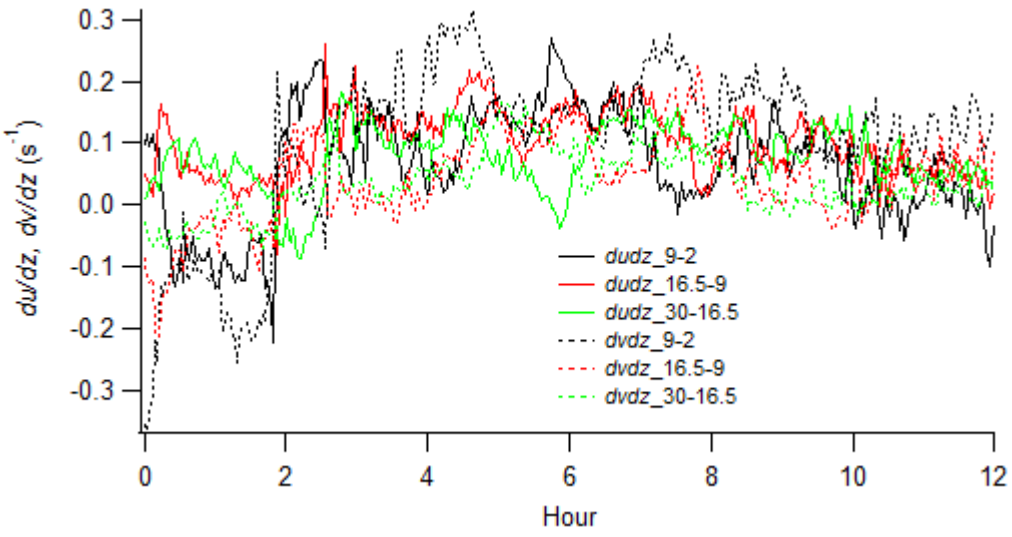

261

262 Figure 12. Vertical wind shears *du/dz* and *dv/dz* over the 2 to 9, 9 to 16.5, and 16.5 to 30 m
263 intervals on October 23.

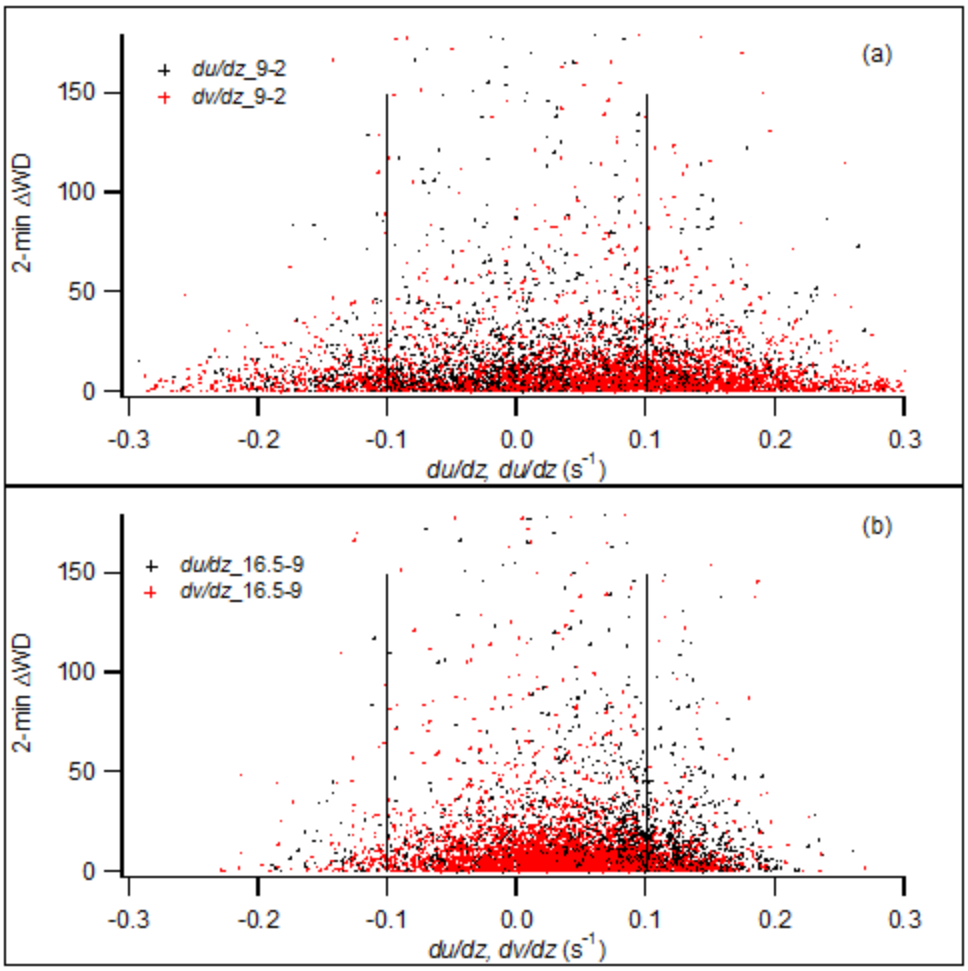

Figure 13. 2-min ΔWD for the aggregated *du/dz* and *dv/dz* wind shears for all time periods included in the analysis for the (a) 2 to 9 and (b) 9 to 16.5 m intervals.

3.4 Relationship of LLJ and W to ΔWD

The presence of LLJ tended to promote wind shear and suppress ΔWD. In Figs. 6-10, parts (b), the heights of where the *U* maxima in LLJ profiles were identified are designated by black 'x'. The *U* maxima associated with each height are designated with red '+'. Most of jet profiles were identified in the sodar data although some weak jet profiles were identified in the sonic data from the tower. All of the test cases shown except October 20 (Fig. 8) had one or more periods where an LLJ was identified. It was not uncommon for the LLJ to intensify with the nose (maximum) lifting in height over an interval of time before dissipating (e.g., Figs. 7, 9).

Parts (c) of Figs. 6-10 indicate that periods with maximum ΔWD activity tended to be associated with relatively quiescent periods of 1-s W. Figure 8(d) shows that this relative quiescence in W was also a feature present across the surface array, not just on the tower.

In contrast, the presence of LLJ was often associated with an increase in W (e.g., Fig. 10, hour 7-12). There are examples where a disturbance in W initiated at 60 m was successively transmitted downward to lower levels, gradually dissipating along the way (Fig. 6, hours 6.5, 8.5). This was in association with LLJ at about 100 m agl. In Fig. 10 it appears as if levels at 30 m and below were affected by the onset of the LLJ with a nose at 50 m agl at about hour 8 with the 60 m level relatively unaffected. By hour 10 when the nose of the LLJ had lifted to over 100 m, W at the 60 m level was maximally affected along the underside of the jet with the effect decreasing downward. Other times the maximal activity in W was mainly at lower levels on the tower even in the presence of LLJ (e.g., Figs. 9, 10).

Many turbulence profiles on GRI showed localized peaks, sometimes in association with wind direction changes between heights (not shown). These peaks were mainly isolated at the intermediate tower levels (9, 16.5, and 30 m). Thus vertical shear was sometimes augmented by lateral directional shear.

3.5 Potential role of gravity waves and other periodic influences on ΔWD

There was little conclusive evidence for a direct causal association between periodic influences and ΔWD. Pressure measurements made at the WSU IRGA sensors as well as some of the 1-s

299 time series of U often suggested the presence of gravity waves with rapid oscillations.
300 Nevertheless, these rapid oscillations could occur with or without corresponding increases in
301 ΔWD and with or without the potential influence of LLJ. Some results from October 23 will be
302 highlighted to illustrate a few of the potential interactions.
303
304 Figure 14 shows time series of 2-min average σ_w and 1-s pressure on October 23. An
305 approximate 1.4 h periodicity in σ_w (and TKE) can be seen with peaks at about 4.7, 6.1, 7.5, and
306 perhaps 9 h. The maxima in σ_w are approximately coincident with local minima in pressure, and
307 vice versa. By reference to Fig. 9a these maxima in σ_w are also approximately coincident with
308 maxima in U. However, there is little in the way of increased ΔWD associated with this (Fig.
309 9b). Note the higher values of σ_w at station ST2, a site that often featured the highest
310 observations of turbulence among the surface stations. It was proximal to a slight upstream
311 terrain undulation.
312
313 On the other hand, Fig. 14 shows a distinct increase in rapid pressure oscillations beginning
314 about hour 10 corresponding to a decrease in U at the surface at hour 9 with the onset of rapid
315 oscillations (Fig. 9a). In this case there appears to be some correspondence between rapid
316 oscillations and increases in ΔWD. Nevertheless, the association might be keyed to the low U
317 rather than the oscillations.
318

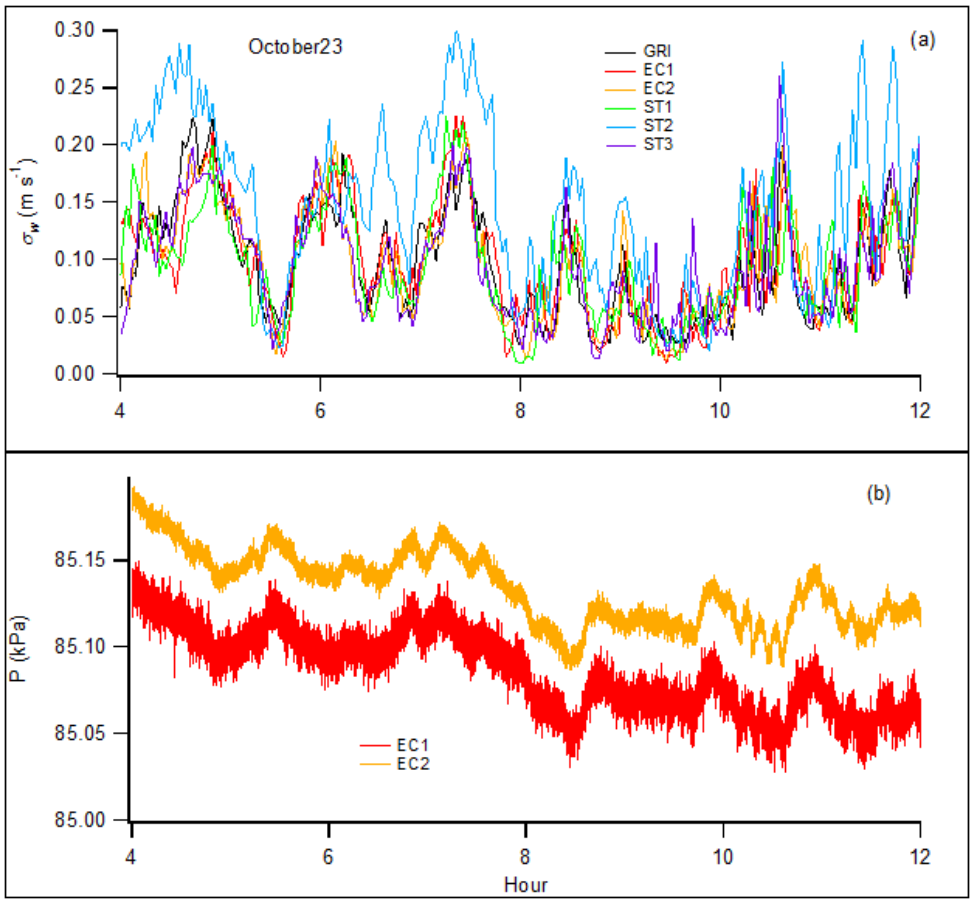

Figure 14. Time series of (a) 2-min average σ_w and (b) 1-s pressure at surface stations, October 23.

4. Discussion

Large and rapid wind direction changes are clearly a common feature in the low U vSBL. The changes can be oscillatory and quasi-periodic with meandering time scales ranging from as little as 5-10 minutes (Mortarini et al. 2016a) up to about a half-hour or more (Hanna 1983; Sun et al. 2012; Mortarini and Anfossi 2015; Mortarini et al. 2016b; Finn et al. submitted). The changes can also be intermittent and highly irregular and unpredictable (Mahrt 2007, 2008). They can alternate unpredictably between periods featuring relative stationarity, periods with regular oscillatory behavior, and periods dominated by very irregular intermittency.

Previous work by Mahrt (2007, 2008) linked wind meander in the nocturnal boundary layer to the strength of mesoscale motions arising from various sources during weak large-scale flows. He found that a ratio of the strength of the mesoscale flow relative to the vector average wind could vary significantly and that large values of this ratio were associated with large standard deviations in wind direction. The variability of this measure was largely unpredictable but appeared to be stronger in more complex terrain and exhibited some correspondence with large vertical shear of wind direction.

Sun et al (2015) described potential mechanisms involving the interactions between waves and turbulence that could contribute to large, abrupt wind direction changes. Sun et al. (2012) have proposed a 3-regime nocturnal turbulence scheme that partly addresses the wind direction observations. In regime 1, U is less than a critical threshold value, turbulence is very weak, and wind directions are more prone to oscillatory behavior. The threshold value is near 1.5 m s^{-1} near the surface and increases with height. In regime 2, U is greater than the threshold and wind direction oscillations are suppressed. Variations in U back and forth below and above the threshold could trigger or suppress, respectively, large changes in wind direction in an irregular manner (their transition A). Much of the data included in the present analysis would be assigned to their regime 1.

Oettl et al. (2005) and Goulart et al. (2007) suggest meandering is a special case of the Navier-Stokes equation at low U in which "equilibrium between Coriolis force and pressure gradient generates a solution that shows oscillatory characteristics". Thus an increase in the horizontal pressure gradient inhibits meandering. Other work has found that the frequency of meander or

355 near meander increased with a decrease in U or increase in stability based upon the ratio between
356 a parameter for the large scale meandering time scale and a parameter for the small scale
357 turbulence time scale at $U < 1.5$ m s^{-1} (Mortarini et al. 2016a, b).
358
359 The present work suggests that most of the rapid, irregular changes in wind direction occur over
360 short periods, often just a few minutes long. These are triggered by the collapse of the turbulent
361 fluxes resulting in complete vertical decoupling. There are several potential mechanisms that
362 could sustain the intermittent turbulent fluxes and mixing and, consequently, coupling (Mahrt
363 2014; Sun et al. 2015; Mortarini et al. 2016a; Lan et al. 2018). Failing that, any turbulent eddies
364 generated are localized and have small enough vertical scales such that they do not interact with
365 the surface (Mortarini et al. 2016a; Lan et al. 2018). This has consequences on the validity of
366 MOST in these conditions (Hicks et al. 2014; Liang et al. 2014; Trini Castelli et al. 2014; Lan et
367 al. 2018).
368
369 These periods of rapid, irregular wind direction change can be sustained over longer periods and
370 rotate through more than 360^{o}. This work also supports a near surface value $U \approx 1.5$ m s^{-1} as a
371 critical threshold value. It is likely that the irregular, intermittent regime is a common state of the
372 vSBL (U at 2m < 1.5 m s^{-1}) with respect to wind direction changes in the absence of some
373 forcing mechanism that imposes some sort of periodicity. Lan et al (submitted) also found the
374 threshold velocity has a height dependency with a value of about 1.6 m s^{-1} near the surface.
375 Consistent with the results reported here, they identified a layer near surface where large wind
376 direction changes were frequent but with relatively constant wind directions above.
377

5. Conclusions

This paper investigated the occurrence and magnitude of rapid, intermittent wind direction changes in the very stable boundary layer. The evidence indicates that these large wind direction changes are largely restricted to near surface wind speeds less than 1.5 m s^{-1} when momentum and sensible heat fluxes approach zero in low wind shear conditions. The magnitude of the wind direction changes is greatest near the surface and generally decreases rapidly upward. The presence of LLJ suppresses the incidence of these wind direction changes. The large wind direction changes occur mainly in weakly turbulent conditions but are otherwise largely independent of the magnitude of turbulence. The evidence was inconclusive to support gravity waves or other periodic behavior as an important triggering mechanism for the rapid, intermittent wind direction changes.

Acknowledgments

We wish to acknowledge Kirk Clawson, Roger Carter, Shane Beard, Brad Reese, Donna Davis, Matt Brewer, and Devin Clinger from the Field Research Division of NOAA and Justine Missik and Raleigh Grysko from the Laboratory for Atmospheric Research at Washington State University for their contributions to the field campaign. Participation by Washington State University was supported by National Science Foundation AGS under Grants #1419614. The scientific results and conclusions, as well as any views or opinions expressed herein, are those of the author(s) and do not necessarily reflect the views of NOAA or the Department of Commerce.

References

Anfossi D, S. Alessandrini, S. Trini Castelli, E. Ferrero, D. Oettl, and G. Degrazia, 2006: Tracer dispersion simulation in low wind speed conditions with a new 2-D Langevin equation system. *Atmos. Environ.* **40**, 7234–7245.

Barad, M. L., Ed., 1958a: Project Prairie Grass, a field program in diffusion: Vol. I of Geophysical Research Papers 59. Air Force Cambridge Research Center Rep. AFCRC-TR-58-235(I), 280 pp. [Available online at http://www.jsirwin.com/PGrassVolumeI.pdf.]

——, 1958b: Project Prairie Grass, a field program in diffusion: Vol. II of Geophysical Research Papers 59. Air Force Cambridge Research Center Rep. AFCRC-TR-58-235(II), 209 pp. [Available online at http://www.jsirwin.com/PGrassVolumeII.pdf.]

Cimorelli, A.J., S.G. Perry, A.Venkatram, J.C. Weil, R.J. Paine, R.B. Wilson, R.F. Lee, W.D. Peters, R.W. Brode, and J.O. Paumier, 2004: AERMOD: Description of model formulation. U.S. Environmental Protection Agency, EPA-454/R-03-004, 91 pp.

Cimorelli, A.J., S.G. Perry, A. Venkatram, J.C. Weil, R.J. Paine, R.B. Wilson, R.F. Lee, W.D. Peters, and R.W. Brode, 2005: AERMOD: a dispersion model for industrial source applications. Part I: general model formulation and boundary layer characterization. *J. Appl. Meteorol*. **44**, 682-693.

Clawson, K.L., R.M. Eckman, N.F. Hukari, J.D. Rich, and N.R. Ricks, 2007. *Climatography of the Idaho National Laboratory, 3rd edition*. NOAA Tech. Memo OAR ARL-259, Air Resources Laboratory, Idaho Falls, ID. 142 pp, doi:10.7289/V500003F

EPA, 2000: Meteorological monitoring guidance for regulatory modeling applications. U.S. Environmental Protection Agency Rep. EPA-454/R-99-005, 171 pp. [Available online at https://www3.epa.gov/scram001/guidance/met/mmgrma.pdf.]

Finn D., K.L. Clawson, R.M. Eckman, R.G. Carter, J.D. Rich, T.W. Strong, S.A. Beard, B.R. Reese, D. Davis, H. Liu, E. Russell, Z. Gao, and S. Brooks, 2015: Project Sagebrush Phase 1, NOAA Technical Memorandum OAR ARL-268, Air Resources Laboratory, Idaho Falls, Idaho, 338 pp. doi: 10.7289/V5VX0DHV

Finn D, K.L. Clawson, R.M. Eckman, H. Liu, E.S. Russell, Z. Gao, S. Brooks, 2016: Project Sagebrush: Revisiting the value of the horizontal plume spread parameter σ_y. *J. Appl. Meteorol. Clim*. **46**, 2019-2037. doi:http://dx.doi.org/10.1175/JAMC-D-0283.1

Finn, D., K.L. Clawson, R.M. Eckman, R.G. Carter, J.D. Rich, B.R. Reese, S.A. Beard, M. Brewer, D. Davis, D. Clinger, Z. Gao, and H. Liu, 2017: Project Sagebrush Phase 2. NOAA Tech. Memo OAR ARL-275, Air Resources Laboratory, Idaho Falls, ID. 392 pp, https://doi.org/10.7289/V5/TM-OAR-ARL-275

Finn, D., R.G. Carter, R.M. Eckman, J.D. Rich, Z. Gao, and H. Liu, 2018: Plume dispersion in low wind speed conditions during Project Sagebrush Phase 2 with emphasis on concentration variability. submitted *Bound.-Layer Meteorol.*

Gifford, F.A., 1961: Use of routine meteorological observations for estimating atmospheric dispersion. *Nuclear Safety* **2**, 47-51.

Goulart, A., G. Degrazia, O. Acevedo, and D. Anfossi, 2007: Theoretical considerations of meandering wind in simplified conditions. *Bound.-Layer Meteorol*. **125**, 279-287.

Hanna, S.R., 1983: Lateral turbulence intensity and plume meandering during stable conditions. *J. Clim. Appl. Meteorol.* **22**, 1424-1430.

Hicks, B. B., W. R. Pendergrass, C. A. Vogel, R. N. Keener, and S. M. Leyton, 2014: On the micrometeorology of the Southern Great Plains 1: Legacy relationships revisited. *Bound.-Layer Meteorol*., **151**, 389-405.

Hiscox, A.L., D.R. Miller, and C.J. Nappo, 2010: Plume meander and dispersion in a stable boundary layer. *J. Geophys. Res.* **115**, D21105, doi:10.1029/2010JD014102

Lan C, Liu H, Li D, Katul GG, Finn D (submitted) Distinct turbulence structures in stable boundary layers with two coupling states. *J Geophys Res – Atmos*

Liang, J., L. Zhang, Y. Wang, X. Cao, Q,. Zhang, H. Wang and B. Zhang, 2014: Turbulence regimes and the validity of similarity theory in the stable boundary layer over complex terrain of the Loess Plateau, China. *J. Geophys. Res*., **119**, 6609-6021.

Luhar, A.K., and P.J. Hurley, 2012: Application of a coupled prognostic model to turbulence and dispersion in light-wind stable conditions, with an analytical correction to vertically resolved concentrations near the surface. *Atmos. Environ*. **51**, 56-66. https://doi.org/10.1016/j.atmosenv.2012.01.046

Luhar, A.K., 2013: Lagrangian particle modeling of dispersion in light winds, *in* Lagrangian Modeling of the Atmosphere, Geophysical Mono. Series 200, American Geophysical Union, pp. 37-51.

Mahrt L., 2007: Weak-wind mesoscale meandering in the nocturnal boundary layer. *Environ. Fluid Mech.* **7**, 331-347.

Mahrt L., 2008: Mesoscale wind direction shifts in the stable boundary-layer. *Tellus A: Dynamic Meteorology and Oceanography* **60**, 700-705.

Mahrt L., 2014: Stably stratified atmospheric boundary layers. *Annu. Rev. Fluid. Mech*. **46**, 23-45. doi:10.1146/annurev-fluid-010313-141354

Mortarini L., and D. Anfossi, 2015: Proposal of an empirical velocity spectrum formula in low-wind speed conditions. *Q. J. R. Meteorol. Soc*. **141**, 85-97. Doi:10.1002/qj.2336

Mortarini L., M. Stefanello, G. Degrazia, D. Roberti, S. Trini Castelli, and D. Anfossi, 2016a: Characterization of wind meandering in low-wind-speed conditions. *Bound.-Layer Meteorol.* **161**, 165-182. doi:10.1007/s10546-016-0165-6

Mortarini L, S. Maldaner, L.P. Moor, M.B. Stefanello, O. Acevedo, G. Degrazia, and D. Anfossi, 2016b: Temperature auto-correlation and spectra functions in low-wind meandering conditions. *Q. J. R. Meteorol. Soc.,* **142**, 1881-1889. doi: 10.1002/qj.2796

Oettl D., A. Goulart, G. Degrazia, and D. Anfossi, 2005: A new hypothesis on meandering atmospheric flows in low wind speed conditions. *Atmos Environ*. **39**, 1739-1748. https://doi.org/10.1016/j.atmosenv.2004.11.034

Sagendorf, J.F., and C.R. Dickson, 1974: Diffusion under low windspeed, inversion conditions. NOAA Tech. Memo. ERL ARL-52, 89 pp. [Available online at http://www.arl.noaa.gov/documents/reports/ARL-52.pdf.]

Slade, D.H., Ed., 1968: Meteorology and Atomic Energy. U.S. Atomic Energy Commission Office of Information Services Rep. TID-24190, 445 pp. [Available online at https://www.orau.org/ptp/PTP%20Library/library/Subject/Meteorology/meteorology%20and%20atomic%20energy.pdf.]

Sun J., L. Mahrt, R. Banta, and Y.L. Pichugina, 2012: Turbulence regimes and turbulence intermittency in the stable boundary layer during CASES-99. *J. Atmos. Sci.* **69**, 338-351. http://dx.doi.org/10.1175/JAS-D-11-082.1

Sun J., L. Mahrt, C. Nappo, and D. Lenschow, 2015: Wind and temperature oscillations generated by wave-turbulence interactions in the stably stratified boundary layer. *J. Atmos. Sci*. **72**, 1484-1503. doi:10.1175/JAS-D-0129.1

Turner, D.B., 1970: Workbook of atmospheric diffusion estimates. U.S. Environmental Protection Agency Office of Air Programs Pub. AP-26, 84 pp. [Available online at http://www.dot.ca.gov/newtech/researchreports/1969-1970/70-07.pdf.]

Trini Castelli S., S. Falabino, L. Mortarini, E. Ferrero, R. Richiardone, and D. Anfossi, 2014: Experimental investigation of surface-layer parameters in low-wind speed conditions in a suburban area. *Q. J. R. Meteorol. Soc*. **140**, 2023-2036. Doi:10.1002/qj.2271

Venkatram A., M.G. Snyder, D.K. Heist, S.G. Perry, W.B. Petersen, and V. Isakov, 2013: Re-formulation of plume spread for near-surface dispersion. *Atmos. Environ*. **77**, 846-855. [http://dx.doi.org/10.1016/j.atmosenv.2013.05.073]

List of Figures

Figure 1. Example 1-s wind direction time series. The wind directions have been rotated from 0 to 360° coordinates to -180° to +180° to minimize frequent wrapping through true north.

Figure 2. Ten-minute average (a) bulk Richardson number (Ri_b) and (b) Brunt-Väisälä frequency (N) for all times used. The starting October dates are indicated in the legend.

Figure 3. Two-minute ΔWD as a function of U at 2 m a.g.l. for all times used.

Figure 4. ΔWD results as a function of the sensible heat and momentum fluxes for all the 2-min periods of Table 1 at four heights on the tower.

Figure 5. ΔWD results as a function of σ_w, √TKE, and σ_T for all of the 2-min periods included in Table 1.

Figure 6. GRI tower October 8: (a) 1-s U and 10-min Ri_b; (b) 2-min ΔWD (-10° offsets for successive heights beginning at 3.7 m) and 10-min LLJ (height and U_{max}); and (c) 1-s vertical velocity W. ΔWD and W traces for adjacent heights are offset for clarity by 10° and 0.4 m s^{-1}, respectively. Hour is time from 1900 MST reference.

Figure 7. GRI tower October 19 with same caption as Fig. 6.

Figure 8. GRI tower October 20: (a) 1-s U and 10-min Ri_b; (b) 2-min ΔWD (-10° offsets for successive heights beginning at 3.7 m) (no LLJ); (c) 1-s vertical velocity W; and (d) 1-sec vertical velocity W measured across surface array. ΔWD and W traces for adjacent heights are offset for clarity by 10° and 0.4 m s^{-1}, respectively. Hour is time from 1900 MST reference.

Figure 9. GRI tower October 23 with same caption as Fig. 6.

Figure 10. GRI tower October 26 with same caption as Fig. 6.

Figure 11. Fraction of 2-min ΔWD changes binned in 5° intervals by (a) height on the GRI tower and (b) the surface array.

Figure 12. Vertical wind shears *du/dz* and *dv/dz* over the 2 to 9, 9 to 16.5, and 16.5 to 30 m intervals on October 23.

Figure 13. 2-min ΔWD for the aggregated *du/dz* and *dv/dz* wind shears for all time periods included in the analysis for the (a) 2 to 9 and (b) 9 to 16.5 m intervals.

Figure 14. Time series of (a) 2-min average σ_w and (b) 1-s pressure at surface stations, October 23.